LAWRENCE
LIVERMORE
NATIONAL
LABORATORY

LLNL-JRNL-645177

Grain boundary energy function for FCC metals

V. Bulatov, B. Reed, M. Kumar

October 24, 2013

Acta Materialia

Disclaimer

This document was prepared as an account of work sponsored by an agency of the United States government. Neither the United States government nor Lawrence Livermore National Security, LLC, nor any of their employees makes any warranty, expressed or implied, or assumes any legal liability or responsibility for the accuracy, completeness, or usefulness of any information, apparatus, product, or process disclosed, or represents that its use would not infringe privately owned rights. Reference herein to any specific commercial product, process, or service by trade name, trademark, manufacturer, or otherwise does not necessarily constitute or imply its endorsement, recommendation, or favoring by the United States government or Lawrence Livermore National Security, LLC. The views and opinions of authors expressed herein do not necessarily state or reflect those of the United States government or Lawrence Livermore National Security, LLC, and shall not be used for advertising or product endorsement purposes.

Grain boundary energy function for FCC metals

Vasily V. Bulatov, Bryan W. Reed, and Mukul Kumar

Lawrence Livermore National Laboratory, Livermore, California 94550, USA

Abstract:

Anisotropy of interfacial energy is the principal driving force for thermally driven microstructure evolution, yet its origins remain uncertain and a quantitative description lacking. We present and justify a concise hypothesis on the topography of the functional space of interface energies and, based on this hypothesis, construct a closed-form function that quantitatively describes energy variations in the 5-space of macroscopic parameters defining grain boundary geometry. The new function is found to be universal for the crystallography class of face-centered cubic metals.

Keywords:

Grain boundary energy; crystal structure; misorientation; modeling; lattice geometry

1. Introduction

Grain boundaries (GB) affect a great many physical, chemical, and mechanical properties of crystalline solids including electrical and thermal conductivity, thermal coarsening, corrosion resistance, impurity segregation, hydrogen embrittlement, stress corrosion cracking, and mechanical strength and ductility [1]. The specific contribution of each given boundary to the material property is largely defined by its excess energy per unit area that depends primarily on boundary geometry or crystallography. The geometric character of a boundary is defined by five macroscopic degrees of freedom (DOFs) that allow several alternative representations, the most common of which is in terms of grain misorientation (three DOFs) plus boundary plane inclination (two more DOFs) [2,3,4]. The GB energy is known to be anisotropic and can vary significantly with both the misorientation and the inclination, especially in face-centered cubic (FCC) metals [5,6,7].

Despite its recognized importance and an extensive body of literature on the subject, both experimental and theoretical, the GB energy anisotropy has not been systematically quantified. Particularly lacking is a sense of the GB energy dependence on plane inclination, which is difficult to quantify experimentally. Reflecting this poor understanding, and with very few exceptions, current models of GB network evolution disregard GB energy anisotropy altogether or account only for the misorientation dependence of the GB energy. Yet, depending on the GB plane orientation, boundaries of the same grain misorientation can have vastly different energies [6,7]. Furthermore, except for nanocrystals in which the grains can rotate, it is precisely the variations of the GB energy with plane inclination – and not misorientation – that define the capillary force driving boundary motion.

Previous attempts to relate the GB energy anisotropy to lattice geometry have been unsuccessful raising legitimate doubts about the very existence of a concise relationship [8]. The primary difficulty stems from the high dimensionality and intricate topology of the “misorientation + inclination” 5-space making it difficult to decouple the inclination-dependent variations from the anisotropy in the misorientation subspace. In addition, for a given set of five macroscopic degrees of freedom, the GB energy depends on translations along the boundary plane (microscopic degree of freedom) and can be affected by various modes of atomic relaxation, e.g. symmetry-breaking atomic reconstructions, free volume re-distribution, etc [1]. Nevertheless, both experimental observations and atomistic calculations reveal certain common and consistent trends in GB energy variations among materials of a given crystallography class (FCC, BCC, etc.) suggesting that lattice geometry does play a role in defining the GB energy anisotropy. Particularly noteworthy are observed close correlations between the GB energy and the spacing between lattice planes parallel to the boundary and the magnitude of the planar unit cell area [9,10,11,12]. Yet the strongest impetus to continue to seek a purely geometric description of the GB energy anisotropy was a recent observation of a close scaling among the energies of 388 geometrically distinct boundaries computed for four FCC metals Ni, Al, Au and Cu [6,7]. The observed scaling suggests that a functional relationship between the GB energy and five geometric DOFs does exist but we do not know what it is.

Existing geometric models relate the GB energy anisotropy to a measure of lattice coincidence [13], plane inter-locking [14], hard-sphere packing [15], excess free volume [9], boundary proximity to symmetric cusp orientations [10,16] and others. While these models capture interfacial energy variations within limited sub-sets of the 5-space, all our attempts so far to extend the same models to the entire sample of 388 boundary geometries have failed, prompting us to consider an entirely different approach. Following [6,7] we assume that the GB energy is a continuous function of five macroscopic DOFs and, thus, the energy of a given boundary can be approximated by interpolation between nearby boundaries with known energies. By itself this proposition is hardly constructive given that many more than 388 samples are needed in order to enable accurate energy interpolation in the entire 5-space ($3^5 \approx 388$). To make interpolation practical it is useful to first grasp the global topography of the energy function in the 5-space. Here we develop an accurate closed-form expression describing variations of interfacial energy in face-centered cubic (FCC) metals as a function of GB geometry. Our approach relates interfacial energy anisotropy to the global topography and connectivity (topology) of the 5-space dominated by special low-dimensional subsets termed *grofs*. The new interfacial energy function uses grofs as scaffolding for hierarchical interpolation providing an accurate description of GB energy anisotropy in four FCC metals in the entire 5-space. Among the numerical parameters defining the GB energy function, only two are found to be metal-specific with the rest held universal for the FCC crystallography class.

The paper is organized as follows. The concept of grofs and the associated general approach of hierarchical interpolation are introduced in section II. Section III describes in detail how hierarchical interpolation is implemented in this particular work for the purpose of describing GB energy variations in the 5-space. The resulting description of GB energy anisotropy is then presented and discussed in section IV. Finally, section V summarizes our findings. The appendix contains a table of numerical best-fit parameters fully defining our interpolation function and describes how to download and use its matlab function for computing the energy of an arbitrary boundary in an FCC metal.

2. General approach

2.1. Topography of interface energy variations in 5D

As a motivation, consider a much simpler yet pertinent example of energy anisotropy among crystal interfaces, namely the variations of surface energy as a function of surface orientation. Neglecting possible near-surface atomic relaxation and surface reconstruction, a simple qualitative model of surface energy anisotropy is obtained by counting the density of first nearest-neighbor (1NN) bonds cut by the surface plane [17,18] in a perfect lattice. A polar plot of the broken 1NN bond density is given in figure 1 for the FCC lattice. Defining the topography of the surface energy variations are six grooves crisscrossing the otherwise smooth energy function. Each groove corresponds to a 1D-set of planes that are parallel to and, thus, do not cut one of the six 1NN bonds in the FCC crystal. Orientations for which two or more such grooves intersect correspond to cusps: that all cusps seen on the figure lie at the intersection of exactly two or three grooves, in ⟨100⟩ and ⟨111⟩ directions, respectively, is a consequence of the symmetry of the FCC lattice.

Our hypothesis is that, just like the surface energy in figure 1, the topography of GB energy function is defined by grooves, i.e., special sub-sets of the 5-space where the energy is minimal with respect to variations locally orthogonal to the set. To avoid confusion with the real physical grooves observed at the intersections of GB with crystal surfaces, we refer to such locally minimal subsets of 5-orientations as *grofs* (from Old Norse gróf for “pit”). A grof of order k or, simply, k-grof of a function in the N-dimensional-space is defined here as a contiguous (N-k)-dimensional subset of the N-space such that most points in the subset possess the following *grof property*: the function is smooth in the (N-k)-subset itself but is a cusp in the complementary k-subspace. As discussed in the following, certain subsets of high-symmetry boundaries appear to be low-energy grofs and are selected as a basis for defining the global topography of the GB energy function.

In the case of surface energy shown in figure 1, there are six distinct 1-grofs and 14 distinct 2-grofs on the 1NN function. In this 2D case, each 2-grof is a true cusp since its dimensionality is zero. Similarly, a 5-grof in the 5-space of GB orientations is a true

cusp. In defining the grofs we stated that most but not all points in a grof set must possess the grof property. This leaves room for possible intersections of two or more grofs. In the 5-space, grof intersections can be grofs of higher order k but not necessarily 5-grofs or true cusps. The grofs are important since, as low-dimensional subsets of orientations with (locally) minimal energies, they define the topography of the energy function in the 5-space. Topology (connectivity) of grofs is defined by crystal symmetries.

If real, the proposed grof topography should greatly simplify interpolation in the 5-space by allowing, at least in principle, to approximate the energies of various boundaries by their proximity to grofs. As a first step, we used the datasets of 388 computed GB energies to identify important grofs of low energy and/or high symmetry. Precise conditions defining energy grofs in the 5-space remain uncertain. On one hand, the excess energy must account for bond distortion related to the degree of lattice coincidence between the two grains (lattice coincidence is commonly quantified by the inverse Σ–number or Σ^{-1} [1,13]). On the other hand, the energy must also depend on the area density of bonds cut (or distorted) by the interface and, thus, on the boundary plane orientation.

Based on the GB energy data presently available, we hypothesize that many rational grain misorientations of high lattice coincidence are 3-grofs (cuspy in the 3-subspace of grain rotations but smooth in the 2-subspace of plane inclinations). Of these, Σ1, Σ3, Σ5, Σ11, and Σ17 grofs will be partially accounted for in the resulting 5D function, whereas all other 3-grofs of this type are deemed too shallow and ignored. Some 1d subsets of *twist boundaries* (for which the rotation axis is perpendicular to the boundary plane) appear to be 4-grofs. In particular, excess energies of all ⟨111⟩-twist boundaries are low because a twist rotation around any of the four ⟨111⟩ axes leaves three 1NN ⟨110⟩ bonds intact (in the boundary plane). Likewise, twist rotations around ⟨110⟩ and ⟨100⟩ axes leave intact one and two 1NN bonds, respectively. Tellingly, the mentioned subsets of symmetric twist boundaries correspond to the three most widely spaced {111}, {100}, and {110} boundary planes with well-documented low energies [10,11,12]. These three high-symmetry 4-grofs are also accounted for in the 5D function. Some of

the grofs intersect. For example, a coherent twin boundary is simultaneously a Σ3 boundary and a ⟨111⟩-twist boundary: this boundary is a true cusp (5-grof).

2.2. Hierarchical interpolation

However impressive, the set of 388 boundaries examined in [6,7] was selected based on criteria favoring high symmetry boundaries of high lattice coincidence (low Σ) and/or with low index boundary planes. Such selection rules generally disfavor GBs vicinal (adjacent) to the high-symmetry subsets and other low-symmetry boundaries, leaving attribution of boundary subsets as grofs somewhat uncertain. At the same time, many of the high-symmetry low-dimensional subsets in the 5-space, including the above mentioned 3- and 4-grofs, are well sampled. Leaving precise attribution of grofs for future work, our present interpolation approach is: (a) quantify and fit the GB energy variations within several well-sampled low-dimensional subsets (preferably grofs) of the 5-space and (b) use the so-fitted subsets as scaffolding onto which the global 5-dimensional interpolation function is stretched. For constructing our interpolation function we opted to use three rotational subsets of highest symmetry: the ⟨100⟩, the ⟨111⟩ and the ⟨110⟩ rotation sets. Here, by a rotation set we mean all possible boundaries that can be produced by a rotation around the set axis. Even though it remains uncertain whether the three selected scaffolding 3D-sets are actually grofs, some of their low-dimensional subsets are nearly certainly grofs. Whatever the case, our particular choice is justified, *postfactum*, by observing that variations of GB energy within each of the three selected scaffolding sets are relatively featureless and simple to parameterize.

To construct a 5D energy function, first we accurately parameterize variations of the GB energy within the three rotational 3D-sets[1]. The approximating 3D-sets are parameterized hierarchically: first in their special 1D sub-sets, then in their 2D sub-sets

[1] Note that these sets are not in general linear vector spaces; in fact it is difficult to define a natural, unambiguous notion of a linear combination in the 5D configuration space. Rather, they are manifolds with nontrivial (and somewhat arbitrary) metrics but well-defined dimensionality. While in some representations (e.g. Rodrigues space) the 1D sub-sets will appear as straight lines, in others (e.g. Euler-angle space), they will not in general.

and finally in the entire 3D-sets. As illustrated in Fig. 2(a), the lower dimensional sub-sets serve as scaffolding for the higher dimensional sub-sets. Once fully parameterized, three rotational sets provide a 3D scaffolding for energy interpolation in the entire 5-space: the energy of a boundary that is not in any of the three scaffolding sets is approximated by the boundary's proximity to the sets. Interpolation can be accurate provided no boundary in the 5-space is too far away from all three scaffolding sets that criss-cross the 5-space. Fortunately, the high symmetry of the cubic lattice enhances the coverage of the 5-space by the three 3D sets. Interpolation between the scaffolding sets requires a measure of distance between the boundaries - a metric in the 5-space. As detailed in the next section, we circumvent the notorious uncertainty in defining such a metric [19,20,21] by using two sub-metrics to evaluate the proximity: one sub-metric in the misorientation 3-space and another sub-metric in the 2-space of boundary plane inclinations.

Fig. 2(b) illustrates topology and symmetries of the 5D space and the scaffolding sets therein. The shaded volume is a representation of the fundamental zone in Rodrigues space [22]. In a cubic crystal, with 24 rotations and 24 rotation-reflections in its point group, one is free to choose a single representation of the misorientation axis-angle pair (ψ, a_x, a_y, a_z) such that ψ is as small as possible and $a_x \geq a_y \geq a_z \geq 0$ (to break ties, such as on the kite-shaped front face, we select the representation with the smaller a_z). Under such rules every possible grain misorientation is represented by a point in the fundamental zone of Rodrigues vector space defined as (a_x, a_y, a_z)tanψ/2 (the shaded truncated tetrahedron in the figure). The boundary plane normal in the frame of grain 1 can be conveniently depicted as a unit vector emanating from the misorientation point, thus capturing all five degrees of freedom in a single representation: a twist boundary will now have its plane normal vector aligned along its Rodrigues vector while a tilt boundary will have its plane normal vector aligned perpendicular to its Rodrigues vector. If desired, one could also add a unit vector representing the boundary plane normal in grain 2, thus improving the symmetry of the representation at the cost of some redundancy. In addition to the $\Sigma 1$ origin (null misorientation) shown in fig. 2(b), other symmetrically equivalent representations of $\Sigma 1$ (e.g. the 90° [100] point shown in the figure) could also be taken as the origin of the coordinate system, thus the same

boundary may sometimes be represented as a twist boundary with respect to one rotation axis and a tilt or mixed boundary with respect to another axis. In fig. 2(b), the red, green, blue, and violet dots and associated unit normal vectors (arrows) give a few examples of boundaries in the 5D space.

Given the cubic symmetry, all boundaries in the three selected scaffolding sets have their Rodrigues vectors aligned along 5 of the 9 edges of the fundamental zone. Three of the five edges (thick black lines) are immediately recognizable as <100>, <110>, and <111> rotation axes from the definition of Rodrigues vectors. The others two (thick blue lines) are extensions of the <110> edges associated with nearby zones (fig. 2(b) shows one such neighboring zone with dashed lines). The entire misorientation space includes 1152 symmetry-equivalent copies of the fundamental zone, each one of them having 5 of its 9 edges lying along the scaffolding sets. The black dot near the center of the fundamental zone depicts the misorientation that is most distant from all of the scaffolding sets: its angular distance d_3 (to be defined later) from the four nearest scaffolding edges is 20.12°. Thus, *all* grain misorientations in a cubic crystal are within 20.12° of some scaffolding set (edge). From an unbiased random sampling of possible misorientations, we estimate that over 53% of all boundaries lie within 10° of at least one of the scaffolding sets. Our interpolation function is constructed as a weighted average of contributions from *all* of the scaffolding sets throughout Rodrigues space (within a cutoff distance, as described in more detail below). This weighted average is dominated by the nearby sets.

The coherent Σ3 twin boundary is a pure-twist 60° [111] boundary, thus its unit normal vector is aligned along the <111> edge of the fundamental zone. Yet the very same boundary is also a symmetric tilt grain boundary obtainable by any of the three distinct <110> rotations; the same purple arrow is simultaneously perpendicular to the three thick blue lines representing the <110> edges of the fundamental zone. This extraordinary symmetry shows why the Σ3 twin is such a special boundary: it lies at the intersection of four distinct low-index rotation sets (which we are taking to be *grofs*) and is either a pure twist or a symmetric tilt boundary in all four. Any deviation from this point, in either misorientation or boundary normal, damages this symmetry. Only the Σ1

null boundary exceeds the Σ3 twin in terms of symmetry.

3. Implementation

In the following subsections we first define three special 3-dimensional sub-sets of the 5-space that form scaffolding for our interpolation function (section 3.1), then proceed to define appropriate measures of distance between a general boundary and a scaffolding 3-set and describe our procedure for finding, within each scaffolding set, a best-matching boundary that is nearest to the general boundary being interpolated (section 3.2), define variables and parameterization of energy variations within the selected scaffolding 3-sets (section 3.3) and finally present our interpolation function in an analytical form (section 3.4).

3.1. Scaffolding sets

Our energy function is based on interpolation between three special subsets of the five-dimensional space (or simply 5-space) that include all boundaries obtainable by rotations about any of the three high-symmetry axes <100>, <110>, and <111>. Each of the three selected scaffolding "sets" is a three-dimensional subset of the full 5-space: any boundary in a given scaffolding set is fully defined by the angle ξ of rotation around the set axis (say [100]) and two additional angles η and ϕ (defined below) that fix the boundary plane inclination.

Each 3-set contains sub-sets of still lower dimensions, such as the subset of pure-twist boundaries for which the misorientation axis is normal to the boundary plane. This latter subset is one-dimensional, fully defined by the rotation angle, ξ. Tilt boundaries are defined as a subset of boundaries for which the rotation axis lies in the plane of the boundary: two tilt angles ξ and η are used to specify a tilt boundary within a given 3-set. The two-dimensional subset of tilt boundaries is further subdivided into symmetric tilt grain boundaries (STGB), with $\eta = 0$ (for such boundaries the boundary plane is a plane of mirror symmetry), and asymmetric tilt grain boundaries (ATGB), with $\eta \neq 0$. The energies of boundaries within the two one-dimensional subsets (twist boundaries and STGBs) are explicitly curve-fit for each 3-set. Then the energies of boundaries in the two-dimensional subsets of ATGBs are interpolated from their corresponding one-

dimensional subsets of STGBs. Finally, boundaries of mixed characters (neither pure twist nor tilt) in each set are further interpolated between their ATGB and pure-twist components. Once the three 3-sets are fully parameterized, the general boundaries with rotation axes other than <100>, <110>, and <111>, are approximated as weighted averages of the energies of the nearest elements in the three scaffolding 3-sets. A schematic showing the set-theoretical relationship among the various boundary subsets in the full 5-space is given in Fig. 2.

3.2. Distance between boundaries and scaffolding sets

To enable interpolation, we need to define distance, i.e., a metric, in the 5-space. A variety of equally useable metrics can be defined, separately, for the 3-subspace of grain misorientations (d_3) [23] and for the 2-subspace of plane inclinations (d_2). For d_3 we follow the definition given in [24] that is re-written below in a different form more convenient for our purposes. Our choice for d_2 will be described in the following. Even though both d_3 and d_2 can be defined separately, it is far from obvious how to combine any two such sub-metrics into a measure of distance in the entire 5-space [24-26]. To avoid ambiguity in mixing the two sub-metrics, we regard the misorientation sub-metric d_3 as the primary measure of distance with the inclination sub-metric d_2 being secondary. Accordingly, for a given boundary A (with misorientation R) and for a given high-symmetry rotation axis [*hkl*] (of type <100>, <110>, or <111>), we first find the rotation R' about [*hkl*] that minimizes the distance d_3 between R' and the actual grain misorientation R. Then, among all boundaries with misorientation R' we find the boundary B that is nearest to A in the inclination 2-subspace (i.e. that minimizes d_2). This specifies a boundary B that is the closest match of A in one of the considered high-symmetry 3-sets <*hkl*>. Thus, we factorize the task of finding boundaries nearest to boundary A: for each scaffolding 3-set we first find which rotation ξ most closely matches A in the misorientation 3-space and then find which particular boundary of misorientation ξ is the closest match of A in the inclination 2-space. We use the energies of the so-matched boundaries as approximations (interpolants) to produce an estimate of the energy of boundary A.

For any given boundary, grain misorientation is represented in the reference frame of one of two grains as a rotation matrix R or, equivalently, as an axis-angle pair (ψ, $\boldsymbol{a}$), which rotates the <100> directions in grain 1 to the <100> directions in grain 2. Because of symmetry, R is actually just one representative of an entire coset $R_i = S_i R$, where S_i are the 24 rotational symmetries of FCC crystals. The boundary is also defined by the boundary plane inclination given by its unit normal vectors $\boldsymbol{n_1}$ and $\boldsymbol{n_2}$ in the reference frames of grains 1 and 2, respectively, related by $\boldsymbol{n_2} = R_i \boldsymbol{n_1}$ (figure 3(a)).

We now wish to approximate a general boundary A by another boundary B obtainable by rotation around one of the selected rotation axes $\boldsymbol{A}_j$ ($\boldsymbol{A}_j$ can be one of three distinct <100> axes or one of four distinct <111> axes or one of six distinct <110> axes). The approximating boundary B is characterized by its axis-angle pair (ξ, $\boldsymbol{A}_j$) (figure 3(b)) or, equivalently, rotation matrix R' and the unit normals $\boldsymbol{m_1}$ and $\boldsymbol{m_2}$ defining the boundary plane, with $\boldsymbol{m_2} = R'\boldsymbol{m_1}$.

We first find which lattice misorientation $R'(\xi)$ obtainable by rotation around axis $\boldsymbol{A}_j$ most closely matches (approximates) misorientation $R(\psi)$ of boundary A. A non-unique but mathematically convenient definition of distance d_3 between two rotations was given in [21] and can be expressed as $d_3 = 2\sin(\delta/2)$, where δ is the angle of product rotation $R'^{-1}(\xi)R(\psi)$ minimized as a function of rotation angle ξ. This is schematically shown as a vector sum in Fig. 3(b), though of course this is only a schematic since the product of two rotations is non-commutative and does not follow the rules of vector addition. Straightforward algebra yields for the minimal distance

$$d_3 = 2\sin\left(\frac{\psi}{2}\right)\left(1 - \left(\boldsymbol{a}\cdot\boldsymbol{A_j}\right)^2\right)^{\frac{1}{2}} \qquad (1)$$

and for the minimizing rotation angle

$$\tan\left(\frac{\xi}{2}\right) = \left(\boldsymbol{a}\cdot\boldsymbol{A_j}\right)\tan\left(\frac{\boldsymbol{\psi}}{\mathbf{2}}\right). \qquad (2)$$

Note that the minimizing rotation specifies not a single best-matching boundary B, but rather an entire 2-set of boundaries with the same misorientation $R(\xi)$ but with different boundary plane inclinations. Our second step is to find, among all such boundaries, the best-matching plane inclination: this is achieved by minimizing an inclination distance

defined here as

$$d_2 = 2 - \boldsymbol{m_1} \cdot \boldsymbol{n_1} - \boldsymbol{m_2} \cdot \boldsymbol{n_2}. \quad (3)$$

The above distance is small when each of the two plane normal vectors $\boldsymbol{n_i}$ of boundary A is nearly parallel to the corresponding plane normal vector $\boldsymbol{m_i}$ of the approximating boundary B (i=1,2). In such cases the so-defined distance d_2 is approximately equal to the one half of the sum of squared angles between the corresponding normal vectors $\boldsymbol{n_i}$ and $\boldsymbol{m_i}$. The best-matching inclination is then obtained by minimizing d_2 as a function of $\boldsymbol{m_i}$. It is straightforward to show that, the pair of plane normals $\boldsymbol{m_i}$ that minimizes d_2 is (not normalized)

$$\boldsymbol{m_1} = [I + R'^{-1}(\xi)R(\psi)]\boldsymbol{n_1}, \boldsymbol{m_2} = [I + R'(\xi)R^{-1}(\psi)]\boldsymbol{n_2}\ . \quad (4)$$

Thus, d_2 reaches its minimal value when normal vector $\boldsymbol{m_1}$ of the approximating boundary points midway between $\boldsymbol{n_1}$ and $R'^{1}(\xi)\boldsymbol{n_2}$ (similarly for $\boldsymbol{m_2}$). The procedure for finding the best-matching inclination is illustrated geometrically in Fig. 3(b), where the residual rotation δ is equally partitioned between two grains to yield two new grain orientations, while orientation of the boundary plane in the laboratory frame remains unchanged. For small δ the two deviation angles approach $\pm\delta/2$.

The above matching procedure is performed for each of the four <111> axes, three <100> axes, and six <110> axes, and for each of the 24 symmetry-related representations of boundary *A*. The resulting list of 13x24 approximating boundaries *B* is culled to remove redundant symmetry-equivalent variations along with any boundaries *B* with distances d_3 to *A* exceeding some pre-defined cutoff distance d_{hkl}^{max}. As will be described in section 3.4, the interpolated boundary energy ϵ is then written as a weighted average of the remaining $\epsilon_{hkl}(B)$ values, with the weights that depend on associated misorientation distances d_3 only.

3.3. Parameterization of energy variations within scaffolding sets

While it is perfectly possible to use $\boldsymbol{m_1}$ (or $\boldsymbol{m_2}$) to specify inclinations of the best-matching approximating boundaries, it is rather more common to express the geometric character of a boundary as either twist, or tilt, or mixed. As shown in Fig. 3(b), the tilt angle ϕ is the angle (taken in the first quadrant) between the rotation axis $\pm\boldsymbol{A_j}$ and the

unit normals $\boldsymbol{m_1}$ (or $\boldsymbol{m_2}$) of the approximating boundary. As defined, $\phi = 0$ for a twist boundary, $\phi = \pi/2$ for a tilt boundary, and ϕ takes on intermediate values for mixed boundaries. While the inclination of a twist boundary is fully defined by the condition $\phi = 0$, one more parameter is needed to define the inclination of the tilt and mixed boundaries.

For non-twist approximating boundaries we find it convenient to introduce two angles θ_1 and θ_2 obtained by projecting $\boldsymbol{m_1}$ and $\boldsymbol{m_2}$ onto a plane perpendicular to $\boldsymbol{A_j}$ (Fig. 3(c)): the two angles are obviously constrained to the total best-matching rotation angle $\xi = \theta_2 - \theta_1$. In order to define an origin and the sense of rotation in the perpendicular planes, for each symmetry axis $\boldsymbol{A_j}$ we define a crystallographic reference direction $\boldsymbol{D_j}$ perpendicular to it; for example, for $\boldsymbol{A_j}$ = [100] we set $\boldsymbol{D_j}$ = [010]. While in principle arbitrary, by convention $\boldsymbol{D_j}$ is always taken to be an axis of (at least) two-fold rotational symmetry. Thus, $\boldsymbol{D_j}$ is a <100> direction when $\boldsymbol{A_j}$ is a <100> or <110> direction, and $\boldsymbol{D_j}$ is a <110> direction when $\boldsymbol{A_j}$ is a <111> direction. The third direction $\boldsymbol{E_j} = \boldsymbol{A_j} \times \boldsymbol{D_j}$ completes a Cartesian coordinate frame associated with axis $\boldsymbol{A_j}$ in which θ_1 and θ_2 are defined as shown on Fig. 3(c). We complete our specification of the boundary inclination for any non-twist boundary by defining a tilt asymmetry angle $\eta = \theta_2 + \theta_1$, which is obviously zero for a symmetric tilt boundary (STGB). By convention, η is also set to zero for all twist boundaries. This way any boundary obtainable by rotation around axis $\boldsymbol{A_j}$ is fully defined by three angles ϕ, ξ and η. To avoid redundancy, we account for the existing symmetries and fold all points in the (η, ξ) plane into a minimal symmetry-equivalent zone as shown in Fig. 4.

Energy variations within each scaffolding 3-set are parameterized hierarchically, starting from their one-dimensional subsets of pure twist and symmetric tilt boundaries, then expanding to the two-dimensional subsets of tilt boundaries, then to the three-dimensional scaffolding sets of <100>, <111> and <110> boundaries.

To describe energy variations within the one-dimensional subsets we use the Read-Shockley-Wolf (RSW) function proposed by D. Wolf [27] as an empirical extension of

the classical Read-Shockley solution for the energy of the low-angle and vicinal boundaries. The RSW function is defined as

$$f_{RSW}(\theta;\theta_{min},\theta_{max},a) = \sin\left(\frac{\pi}{2}\frac{\theta-\theta_{min}}{\theta_{max}-\theta_{min}}\right)\left(1 - a\log\sin\left(\frac{\pi}{2}\frac{\theta-\theta_{min}}{\theta_{max}-\theta_{min}}\right)\right), \qquad (5)$$

on segment [θ_{min}, θ_{max}] over which it ranges from 0 to 1 and has an infinite slope at θ_{min} and a slope of zero at θ_{max}. Within these limitations, the dimensionless shape parameter *a* can be used to modify the shape of the RSW function for various applications. For most of our curve fits we find *a* = 1/2 to be satisfactory. We use this latter value of *a* except where otherwise noted: the fitting results are rather insensitive to *a* in part because the set of 388 boundaries has relatively few vicinal boundaries whose energies are sensitive to the values of *a*. The RSW function is convenient for approximating energy variations within one-dimensional subsets of pure twist and symmetric tilt boundaries within the <100>, <110>, and <111> scaffolding 3-sets. These six functions stitch together appropriate RSW functions as shown in Fig. 5. The same figure also lists all the parameters defining the one-dimensional functions.

The two-dimensional subsets of all (symmetric + asymmetric) tilt boundaries are linearly interpolated between the one-dimensional symmetric-tilt subsets for <100> and <110>:

$$\epsilon_{100}^{tilt}(\xi,\eta) = \begin{cases} \epsilon_{100}^{stgb}\left(\frac{\pi}{2}-\xi\right) + \left(\epsilon_{100}^{stgb}(\xi) - \epsilon_{100}^{stgb}\left(\frac{\pi}{2}-\xi\right)\right)\left(1-\frac{2\eta}{\pi}\right)^{p}, \epsilon_{100}^{stgb}(\xi) > \epsilon_{100}^{stgb}\left(\frac{\pi}{2}-\xi\right) \\ \epsilon_{100}^{stgb}(\xi) + \left(\epsilon_{100}^{stgb}\left(\frac{\pi}{2}-\xi\right) - \epsilon_{100}^{stgb}(\xi)\right)\left(\frac{2\eta}{\pi}\right)^{p}, \text{otherwise} \end{cases} \qquad (6)$$

$$\epsilon_{110}^{tilt}(\xi,\eta) = \begin{cases} \epsilon_{110}^{stgb}\left(\frac{\pi}{2}-\xi\right) + \left(\epsilon_{110}^{stgb}(\xi) - \epsilon_{110}^{stgb}\left(\frac{\pi}{2}-\xi\right)\right) f_{RSW}(1-\frac{\eta}{\pi}, a_{110}^{atgb}), \epsilon_{110}^{stgb}(\xi) > \epsilon_{110}^{stgb}\left(\frac{\pi}{2}-\xi\right) \\ \epsilon_{110}^{stgb}(\xi) + \left(\epsilon_{110}^{stgb}\left(\frac{\pi}{2}-\xi\right) - \epsilon_{110}^{stgb}(\xi)\right) f_{RSW}(\frac{\eta}{\pi}, a_{110}^{atgb}), \text{otherwise} \end{cases}$$

.

(7)

This approach was found to be less effective for the two-dimensional set of <111> tilt boundaries that intersect the deep Σ3 grof. The latter grof appears to be well

approximated by an RSW function with a cusp at $\xi = \pi/3$, however there is no evidence in the available data for any η dependence of the <111> tilt energy for low values of ξ. Thus we define,

$$\epsilon_{111}^{tilt}(\xi,\eta) = \begin{cases} \epsilon_{111}^{stgb,max} f_{RSW}\left(\xi; 0, \xi_{111}^{tilt,max}, \frac{1}{2}\right), \xi \leq \xi_{111}^{tilt,max} \\ \epsilon_{111}^{stgb,\Sigma 3}(\eta) + (\epsilon_{111}^{stgb,max} - \epsilon_{111}^{stgb,\Sigma 3}(\eta)) f_{RSW}\left(\xi; \frac{\pi}{3}, \xi_{111}^{tilt,max}, \frac{1}{2}\right), \text{otherwise} \end{cases}, \tag{8}$$

where

$$\epsilon_{111}^{stgb,\Sigma 3}(\eta) = \epsilon_{111}^{stgb,\Sigma 3} + \left(\epsilon_{111}^{atgb,\Sigma 3,max} - \epsilon_{111}^{stgb,\Sigma 3}\right) f_{RSW}\left(\eta; 0, \frac{\pi}{2\lambda}, \frac{1}{2}\right) \tag{9}$$

is the curve fit along the Σ3 grof. This introduces several additional fit parameters, including $\epsilon_{111}^{stgb,max}$, $\xi_{111}^{tilt,max}$, $\epsilon_{111}^{stgb,\Sigma 3}$, $\epsilon_{111}^{atgb,\Sigma 3,max}$, and a scaling parameter λ that allows to account for the different shapes of the Σ3 grof in low stacking fault energy (SFE) and high SFE materials.

The three-dimensional scaffolding sets of mixed - neither tilt nor twist - boundaries are built by interpolation between their twist and asymmetric tilt sub-sets as follows:

$$\epsilon_{hkl}(\xi,\eta,\phi) = \epsilon_{hkl}^{twist}(\xi)\left(1 - \frac{2\phi}{\pi}\right)^{p_{hkl}^1} + \epsilon_{hkl}^{tilt}(\xi,\eta)\left(\frac{2\phi}{\pi}\right)^{p_{hkl}^2} \tag{10}$$

for *hkl* = <100> and <110>, and as a parabola for *hkl* = <111>

$$\epsilon_{111}(\xi,\eta,\phi) = \epsilon_{111}^{twist}(\xi)\left(1 - \alpha\frac{2\phi}{\pi} + (\alpha - 1)\left(\frac{2\phi}{\pi}\right)^2\right) + \epsilon_{111}^{tilt}(\xi,\eta)\left(\alpha\frac{2\phi}{\pi} - (\alpha - 1)\left(\frac{2\phi}{\pi}\right)^2\right) \tag{11}$$

The variables p_{hkl}^1, p_{hkl}^2, and α are fit parameters.

3.4. Full interpolation function

The energy ε of an arbitrary boundary in the 5-space is approximated as a weighted average over the energies ϵ_{hkl} all best-matching boundaries found within the three scaffolding 3-sets:

$$\epsilon = \frac{1+\sum w_{hkl}(d_3)\epsilon_{hkl}(\xi,\eta,\phi)}{1+\sum w_{hkl}(d_3)}\epsilon_{RGB}, \quad (12)$$

where ϵ_{RGB} is the energy of a hypothetical random boundary. The above interpolation function allows a single best-matching boundary to be counted more than once towards the weighted average. However, to reduce multiple counting we remove symmetry-redundant representations of the same boundary as well as representations that are too distant to any of the three 3-sets ($d_3 > d^{max}$). The weighting function is

$$w_{hkl}(d_3) = \frac{w^0_{hkl}}{\sin\frac{\pi d_3}{2d^{max}_{hkl}}(1-\frac{1}{2}\log\sin\frac{\pi d_3}{2d^{max}_{hkl}})-1} \quad (13)$$

where *hkl* is one of <100>, <110>, or <111>. This weighting function is again of the RSW type and describes the energies of boundaries vicinal to one of the scaffolding sets, i.e. for which one of the distances d_3 is much smaller than the other distances. In order to keep the interpolation weights finite, we set $w_{hkl}(d_3)$ equal to some large but finite value when d_3 is numerically close to zero. We re-define all energy parameters in the $\varepsilon_{hkl}(\xi, \eta, \phi)$ functions to be dimensionless expressing them as fractions of ϵ_{RGB} which defines the overall energy scale and is the only parameter with the dimension of energy.

4. Results and Discussion

In all, our function contains 43 numerical parameters - one dimensioned parameter (ε_{RGB}) and 42 dimensionless parameters referred to as ***P*** (a 42-vector) – introduced to describe GB energy variation over five-dimensional space for a single element. These parameters are listed in Table A1 for all four elements, with parameters 2 through 43 making up a vector ***P*** that encodes the *shape* of the function, as opposed to parameter 1 that encodes its *scale*. At first we used these 43 parameters to fit the sets of 388 boundary energies separately for each of four metals. This captured most of the reliable variance in the four data sets, reducing the residual RMS error to 5% (reduced χ^2 ranging from 0.90 to 1.16 for the four elements with an assumed 5% error in all MD-calculated values). The resulting fits revealed several relationships between the sets of best-fit parameters obtained for the four metals. First, within errors derived from the χ^2 analysis, 27 out of 42 components of the four best-fit vectors ***P*** obtained separately for

the four metals were found to be very nearly the same. Second, from principal component analysis on the set of four ***P*** vectors we found that up to 97% of the inter-element variance in ***P*** could be captured with a single scalar parameter that describes the linearly coordinated motion of the remaining 15 elements of ***P***.

These insights prompted us to re-define our interpolation function as universal, with just two material-specific parameters, and re-fit it to all 388 x 4 = 1552 available boundary energies. For that we fix 27 elements of ***P*** to be the same across the four elements and retain a single scalar parameter to describe the inter-element variations in ***P*** while neglecting all other principal components. Thus, our universal function contains only two material-dependent parameters: ϵ_{RGB} and one additional dimensionless parameter to account for the observed linearly coordinated variations in 15 out of 42 elements of ***P***. Given their linear dependence, any of the 15 parameters can be used as the master degree of freedom. To describe the inter-element variations in ***P*** we introduce a single coordinate Φ

$$\boldsymbol{P}(\Phi) = \boldsymbol{P}_{Al} + (\boldsymbol{P}_{Cu} - \boldsymbol{P}_{Al})\Phi \ . \tag{14}$$

As defined in (14), parameter Φ is zero for Al and 1 for Cu.

With the energy function re-defined as universal, a global search was performed to obtain the best-fitting set of numerical parameters using all four datasets containing 388x4 = 1552 boundary energies. In total, our universal energy function contains 63 parameters, including ϵ_{RGB} for all four elements, Φ_{Au}, Φ_{Ni}, $\boldsymbol{P}_{Al}$ (with 42 components), and the 15 elements of $\boldsymbol{P}_{Cu}$ that differed from the corresponding elements of $\boldsymbol{P}_{Al}$. The results of the global fit are shown in Figures 6, 7, 8 and 9. Assuming again a 5% random error across all four atomistic datasets, the total value of χ^2 increased by an insignificant amount compared to the values obtained in four independent fits (one for each element). At the same time, despite a significant reduction in the number of fitting parameters from 43 x 4 = 172 to 63, the reduced χ^2 of 0.984 obtained in the global fit is even lower than the average reduced χ^2 obtained in the four independent fits. This effectively means that there is no loss of statistically significant information even when of the inter-element variations are described with just two parameters instead of 43.

To test the robustness of our fitted function with respect to the choice of GB ensemble, we re-fited it to a reduced dataset of GB energies obtained by removing the 35 worst fitting boundaries, namely the ones for which the fit residual was more than 10% for at least one of the four chemical elements. In general, these 35 boundaries are far from the nearest scaffolding set.and, when included in the fit, account for over 40% of the χ^2. Refitting the function to the so-reduced GB energy data set shifted the fit parameters by a root-mean-square (RMS) value of 1.2 standard deviations which is somewhat significant but unsurprising given the deliberate bias in the selection of the excluded boundaries. At the same time, in comparing the reduced-dataset fit to the function fitted to the entire dataset, the predicted energies of individual boundaries changed insignificantly: an RMS fractional change of 1.2% was observed for the 353 retained boundaries and 1.8% for the 35 removed boundaries - both of which are small compared to the assumed 5% error in the raw GB energy data. In other words, deliberately eliminating from the fitting dataset 35 most atypical boundaries still produces an interpolation function that estimates the energies of those 35 boundaries with a precision comparable to the function fitted to the entire dataset.

Parameter Φ defines inter-element variations in the shape of the five-dimensional interpolation function and can be thought of as the element's position on a hypothetical aluminum-copper axis. This parameter correlates most strongly with the ratio of the coherent twin energy to ϵ_{RGB} (this ratio is shown as ϵ_{twin} in Table A1). Note that ϵ_{twin} appears twice in Fig. 5, since a coherent twin boundary is simultaneously a <110> tilt and a <111> twist boundary.

As can be seen by comparing the curves for Al and Au, the shapes of which (as opposed to the scale) are determined solely by the value of Φ, we see that changes in Φ have some more subtle effects, e.g. affecting the shape of the <111> twist, <111> tilt, and <100> twist sub-sets. The curve fit described below ultimately yielded values of Φ = 0.768 ± 0.022 and Φ = 0.784 ±0.022 for Ni and Au meaning that, apart from an overall scaling factor, the GB energy anisotropy for Ni and Au is nearly the same which could be expected, as an afterthought, given the narrow scatter of energy values for Au as seen in Fig. 9.

The set of 63 best-fit parameters obtained in the global fit is given in Table A1 in the Appendix along with the estimated errors derived from the square roots of the diagonal elements of the inverse of the χ^2 curvature matrix [28]. Such analyses can artificially inflate some of the parameter errors, especially in the (probably frequent) cases where the effects of changing one parameter can be partially compensated by changes in one or more other parameters. Thus, the errors shown in Table A1 should not be regarded as statistically independent.

There is no claim of uniqueness of the function reported here. Many minor variations of the functional form were experimented with during the development cycle and what is reported is the best result so far in terms of the total reduced χ^2 across the set of four elements obtained with a function with just two element-specific parameters. However, several other functional forms (e.g. with RSW functions replaced with power laws or trigonometric functions in some places, or using different weighted-average schemes (equation 13) produced results that were almost as good, with reduced χ^2 values insignificantly larger than the value we report. In any case, the χ^2 analysis shows that our functional form reduces the residual error to essentially random noise, assuming (as is consistent with the scatter plot shown in Fig. 9) that the calculated energies in the four datasets have a 5% RMS random error. Thus, while marginal improvements can still be made (for example, in the functional form for low-angle <110> STGBs, which were problematic for the case of Al), significant further progress demands more data, either for additional FCC elements or for boundaries beyond the existing datasets of 388 boundaries. Of particular value would be additional data on the energies of vicinal boundaries and low-symmetry boundaries that are poorly represented in the current ensemble.

5. Summary

We have presented a novel approach to describing variations of grain boundary energy in FCC metals in the entire 5-space of geometric parameters. Our approach is that of hierarchical interpolation in which the full 5D energy function is built on a scaffolding consisting of lower dimensional sub-sets of the 5-space. The selection of scaffolding is based on the concept of grofs introduced here as special sub-sets of the 5-space where

the energy is locally minimal with respect to variations orthogonal to the grof. The resulting interpolation function is closed-form and accurately describes GB energy anisotropy in four FCC metals Ni, Al, Cu and Au for which data from atomistic simulations is available. Furthermore, except for two element-specific parameters, all other parameters defining the interpolation function are found to be the same for all for metals.

That it is possible to capture the global 5D topography of the GB energy using a universal function with just two metal-specific parameters is a significant reduction in complexity. To the extent that the proposed energy function is indeed universal for FCC metals, one needs to measure or compute just two GB energies, e.g. that of the $\Sigma 3$ coherent twin boundary and one of the high energy random boundaries, to fully define the GB energy anisotropy for a given FCC material in the entire 5-space.

The function reported in this paper was motivated in part by the availability of prior data from atomistic simulations as well as the need to accurately capture the energy spectrum in grain boundary engineered FCC materials, where there is a preponderance of $\Sigma 3$ twin boundaries and its variants, $\Sigma 9$ and $\Sigma 27$. A more comprehensive accounting of the entire phase space of GB geometries will be a natural extension of this work and could include a more thorough exploration of boundaries that can be considered "random" as well as the implied smoothness of the energy landscape.

The 5D energy function presented above is implemented in a MATLAB® code available for download at http://xxx.llnl.gov. The calling sequence of the code is explained in the Appendix.

6. Acknowledgements

This work was performed under the auspices of the US Department of Energy by Lawrence Livermore National Laboratory under Contract W-7405-Eng-48. The authors were supported by the US DOE Office of Basic Energy Sciences, Division of Materials Sciences and Engineering. We are indebted to D. Olmsted for many useful discussions and to L. Zepeda-Ruiz, T. Oppelstrup, and J. Mason for their advice on various technical aspects of this work.

Prepared by LLNL under Contract DE-AC52-07NA27344.

7. Literature

1. A. P. Sutton, R. W. Balluffi, Interfaces in Crystalline Materials, Oxford University Press, Oxford, 1997, pp. 349-352.
2. D. G. Brandon, B. Ralph, S. Ranganathan, M. S. Wald, Acta Metall. 12 (1964) 813.
3. W. Bollman, Crystal Defects and Crystalline Interfaces, Springer-Verlag, Berlin, 1970, pp. 1-14.
4. D. Wolf, J. Phys. 46 (1985) 197.
5. G. S. Rohrer, J. Mater. Sci. 46 (2011) 5881.
6. D. L. Olmsted, S. M. Foiles, E. A. Holm, Acta Mater. 57 (2009) 3694.
7. E. A. Holm, D. L. Olmsted, S. M. Foiles, Scripta Mater. 63 (2010) 905.
8. A. P. Sutton, R. W, Balluffi, Acta Metall. 35 (1987) 2177.
9. D. Wolf, S. Yip, Materials interfaces, Springer, New York, 1992, pp. 87-150.
10. D. Wolf, Acta Metall. 38 (1990) 791.
11. D. Wolf, J. Appl. Phys. 68 (1990) 3221.
12. D. Wolf, Acta Metall. 37 (1989) 1983.
13. W. Bollmann, Philos. Mag. 16 (1987) 363.
14. H. J. Fecht, H. Gleiter, *Acta. Metall*. **33** (1985) 557.
15. M. F. Ashby, F. Spaepen, S. Williams, Acta Metall. 26 (1978) 1647.
16. P. Wynblatt, M. Takashima, Interface Sci. 9, 265 (2001) 273.
17. L. D. Landau, Collected Papers, Pergamon, Oxford, 1971, pp. 540-545.
18. Y. M. Lee, H. I. Aaronson, Acta Metall. 28 (1980) 539.
19. J. W. Cahn, J. E. Taylor, *J. Mater. Sci.* **41** (2006) 7669.
20. A. Morawiec, Acta Mater. 48 (2000) 3525.
21. D. L. Olmsted, Acta Mater. 57 (2009) 2793.
22. U. F. Kocks, C. N. Tomé, H.-R. Wenk, Texture and Anisotropy: Preferred Orientations in Polycrystals and their Effect on Materials Properties, Cambridge University Press, chap. 2.
23. D. Q. Huynh, J. Math. Imaging & Vis. 35 (2009) 155.
24. D. L. Olmsted, Acta Mater. 57 (2009) 2793.
25. J. W. Cahn, J. E. Taylor, *J. Mater. Sci.* **41** (2006) 7669.

26. A. Morawiec, Acta Mater. 48 (2000) 3525.
27. D. Wolf, Scripta Metall. 23 (1989) 1713.
28. P. R. Bevington, Data Reduction and Error Analysis for the Physical Sciences, McGraw-Hill, New York, 1969, pp. 222-246

APPENDIX

Table A1: All of the parameters for the global curve fit on all four elements. Parameter 1 is the over-all energy scale and is an independent parameter for each element. Parameters 2 through 43 constitute the dimensionless vector ***P***. 27 of the elements of ***P*** are held constant for all four elements, while the other 15 are taken to vary linearly with a single element-dependent parameter Φ (equation 14). Uncertainties are included for the 63 independent parameters varied in the global fit.

Number	Name	Description	Ni	Al	Au	Cu
1	ϵ_{RGB}	Random boundary energy, J/m^2	1.445±0.032	0.547±0.012	0.530±0.012	1.037±0.023
2	d_{100}^{max}	Cutoff distance for 100	0.405±0.026			
3	d_{110}^{max}	Cutoff distance for 110	0.739±0.025			
4	d_{111}^{max}	Cutoff distance for 111	0.352±0.025			
5	w_{100}^{0}	Weight for 100 set	2.40±0.60			
6	w_{110}^{0}	Weight for 110 set	1.35±0.12			
7	w_{111}^{0}	Weight for 111 set	2.676	0.352±0.250	2.726	3.38±0.85
8	p_{100}^{1}	100 tilt/twist mix power law	0.602±0.038			
9	p_{100}^{2}	100 tilt/twist mix power law	1.581±0.071			
10	$\epsilon_{100}^{twist,max}$	Maximum 100 twist energy	0.684	0.596±0.017	0.686	0.710±0.018
11	a_{100}^{twist}	Shape factor for 100 twist	0.871	1.310±0.064	0.861	0.738±0.037
12	p	100 ATGB interpolation power law	3.2±1.3			
13	$\epsilon_{100}^{stgb,max1}$	100 STGB energy, first peak	0.893±0.022			
14	$\epsilon_{100}^{stgb,\Sigma5,1}$	100 STGB energy, first Σ5	0.835±0.024			
15	$\epsilon_{100}^{stgb,max2}$	100 STGB energy, second peak	0.933±0.026			
16	$\epsilon_{100}^{stgb,\Sigma5,2}$	100 STGB energy, second Σ5	0.896±0.022			
17	$\epsilon_{100}^{stgb,\Sigma17}$	100 STGB energy, Σ17	0.775±0.018			
18	$\xi_{100}^{stgb,max1}$	100 STGB angle of first peak	0.482	0.392±0.025	0.484	0.510±0.020
19	$\xi_{100}^{stgb,max2}$	100 STGB angle of second peak	0.783±0.114			
20	p_{110}^{1}	110 tilt/twist mix power law	0.743	0.679±0.025	0.744	0.762±0.024
21	p_{110}^{2}	110 tilt/twist mix power law	1.115	1.147±0.062	1.114	1.105±0.051

22	$\xi_{110}^{twist,max}$	110 twist energy peak angle	0.529±0.019			
23	$\epsilon_{110}^{twist,max}$	110 twist energy peak value	0.909±0.022			
24	$\epsilon_{110}^{twist,\Sigma 3}$	110 twist Σ3	0.664±0.020			
25	$\epsilon_{110}^{twist,90}$	110 twist 90 degree (symmetry point)	0.597±0.026			
26	a_{110}^{atgb}	110 ATGB RSW shape factor	0.200±0.055			
27	$\epsilon_{110}^{stgb,max3}$	110 STGB energy of third peak	0.826±0.018			
28	ϵ_{twin}	110 STGB energy Σ3 (coherent twin)	0.043	0.111±0.005	0.042	0.0226±0.0012
29	$\epsilon_{100}^{stgb,max2}$	110 STGB energy of second peak	0.664±0.016			
30	$\epsilon_{100}^{stgb,\Sigma 11}$	110 STGB energy Σ11	0.285	0.242±0.012	0.286	0.298±0.011
31	$\epsilon_{100}^{stgb,max1}$	110 STGB energy of first peak	0.683	0.736±0.025	0.681	0.666±0.017
32	$\pi - \xi_{110}^{stgb,max3}$	110 STGB position of third peak	0.515±0.013			
33	$\pi - \xi_{110}^{stgb,max2}$	110 STGB position of second peak	1.738±0.020			
34	$\pi - \xi_{110}^{stgb,max1}$	110 STGB position of first peak	2.779	3.047±0.066	2.773	2.698±0.025
35	α	111 tilt-twist interpolation (linear if 1)	1.851	1.490±0.124	1.858	1.960±0.059
36	a_{111}^{twist}	111 twist RSW shape factor	0.883	0.665±0.101	0.888	0.949±0.073
37	$\xi_{111}^{twist,max}$	111 twist peak angle	0.495±0.017			
38	$\epsilon_{111}^{twist,max}$	111 twist energy at peak	0.347	0.495±0.016	0.344	0.302±0.009
39	$\xi_{111}^{tilt,max}$	111 ATGB peak angle	0.550	0.469±0.021	0.551	0.574±0.015
40	$\epsilon_{111}^{stgb,max}$	111 ATGB maximum energy	0.837±0.019			
41	$\epsilon_{111}^{stgb,\Sigma 3}$	111 STGB Σ3 energy	0.619±0.020			
42	$\epsilon_{111}^{atgb,\Sigma 3,max}$	111 ATGB Σ3 symmetry point energy	0.845±0.143			
43	λ	111 ATGB mixing η scale factor	0.275	1.0±1.0	0.259	0.049±0.057
	Φ	Element-dependent shape factor	0.768±0.022	0	0.784±0.022	1

Computing grain boundary energies in MATLAB

On xxx.llnl.gov we post a set of MATLAB functions, in the form of '.m' files, that calculate the energy of any given grain boundary in one of the four FCC metals Ni, Al, Au, Cu or in any other user-defined FCC material. The boundary should be represented as a pair of orthonormal rotation matrices *P* and *Q* whose rows specify orientation of the

laboratory (sample) frame in the cube coordinates of crystal grains 1 and 2, respectively. The top row in each matrix defines the orientation of the boundary plane normal written in the two cube frames. The calling sequence for computing the interpolated GB energy should be, for example:

```
[geom100,geom110,geom111] = distances_to_all_sets(P,Q);  % Generate geometry parameters

par43 = makeparvec('Ni');                    % Generate 43-element parameter vector for nickel

en = weightedmeanenergy(geom100,geom110,geom111,par43);          % Calculate the energy
```

The function 'makeparvec' contains four parameters that by default will revert to the values obtained by curve fitting to the full set of 4 elements (i.e. the values in Table A1). The first parameter, 'AlCuparameter', is either a numeric scalar (in which case it is interpreted as the parameter Φ in equation (14)) or a character string (in which case it is interpreted as the symbol for one of the four elements Ni, Al, Au, or Cu). The second parameter is the energy of random boundary e_{RGB} in J/m^2 and defaults to the value for copper. The third and fourth parameters are the 42-element vectors $\boldsymbol{P_{Al}}$ and $\boldsymbol{P_{Cu}}$, also from equation (14). Calling 'makeparvec' with no parameters returns the parameter set for copper.

The above functions call several other functions also supplied on the website: 'distances_to_all_sets' calls 'distances_to_set' that calculates the geometrical parameters for one of the sets <100>, <110>, and <111>. 'weightedmeanenergy' calls functions with specific curve fits to each set, called 'set100', 'set110', and 'set111', and these in turn call the general-use function 'rsw'.

Figure captions

Figure 1: Density of broken 1NN bonds as a function of plane orientation.

Figure 2. a. An illustration of the set-theoretical relationship among the scaffolding sets. Dimensionality of each scaffolding set is given in parentheses. Special subsets of lower dimensionality are wholly included in the more general subsets of higher dimensionality. The subset of $\Sigma 3$ boundaries is the intersection of 111 and 110 sets: the small black circle within this subset is the $\Sigma 3$ (111)/(111) coherent twin boundary. All sets displayed in the figure also intersect at the $\Sigma 1$ "zero misorientation" boundary (not shown). **b.** Geometry of an arbitrary boundary in the 5D space can be represented as a point in Rodrigues space (representing the misorientation) with an attached unit vector (representing the boundary plane normal). We show four examples, superposed on the fundamental zone for misorientations in centrosymmetric cubic crystals. The scaffolding sets lie along the thick black and blue lines. The most remote point from the scaffolding sets is shown near the center of the fundamental zone.

Figure 3: Geometry of grain boundaries: **a.** The axis-angle representation (ψ, $\boldsymbol{a}$) of the rotation and the boundary plane unit normal vectors $\boldsymbol{n_1}$ and $\boldsymbol{n_2}$ in each grain's reference frame; **b.** Finding the best match for boundary A among all boundaries obtainable by rotation about special axis $\boldsymbol{A_j}$. The closest match (ξ, $\boldsymbol{A_j}$) to the exact misorientation (ψ, $\boldsymbol{a}$) leaves a discrepancy that can be represented by a rotation over a small angle δ. Leaving the boundary plane fixed in the lab frame, each grain is rotated by approximately $\pm\delta/2$, defining new approximate grain orientations 1' and 2' with unit normals $\boldsymbol{m_1}$ and $\boldsymbol{m_2}$ expressed in the reference frames of these two grains; **c.** A Cartesian coordinate system ($\boldsymbol{A_j}$, $\boldsymbol{D_j}$, $\boldsymbol{E_j}$) is defined in a crystallographic reference frame, e.g. ($\boldsymbol{A_j}$, $\boldsymbol{D_j}$, $\boldsymbol{E_j}$) = ([100],[010],[001]) for each axis $\boldsymbol{A_j}$. $\boldsymbol{D_j}$ is always chosen to be a <100> or a <110> direction. The boundary plane normals in the approximating boundary are projected into the ($\boldsymbol{D_j}$, $\boldsymbol{E_j}$) plane, thus defining the angles θ_1 and θ_2.

Figure 4: Variable transformation from (θ_1, θ_2) to (ξ, η) and reduction to a minimal symmetry-equivalent triangular zone (union of light gray and dark gray regions). By symmetry, all functions must be periodic in θ_1 and θ_2 with period *p* and possess mirror symmetry with respect to the ξ and η axes. The point marked with a dot has 2-fold rotation symmetry, thus the boundary segment shown in a dashed line is redundant. All other boundary segments are parts of the shaded irreducible zone. Twist boundaries are defined to have η = 0. While such symmetry reduction is applicable to all high-symmetry axes, the set of <111> tilt boundaries possesses an extra symmetry reducing the fundamental zone to the dark gray region.

Figure 5: Parameterization of GB energy variations within special one-dimensional subsets of twist and symmetric tilt boundaries in the <100>, <110>, and <111> scaffolding sets. Numerical parameters (angles and scaled energies) defining the shapes of the one-dimensional functions are listed on the plots. Unless shown on the plot, parameters *a* defining the shape of the RSW functions are set to *a* = 0.5.

Figure 6: GB energy variations in low-dimensional subsets within the 100 rotational set. The symbols are energies taken from the datasets of 388 boundaries with the assumed error bars of 5% while the lines and the surface shows the fit function itself. (**A**) Energies of twist boundaries as a function of rotation angle. (**B**) Energies of symmetric tilt boundaries as a function of rotation angle. (**C**) Energies of all tilt (symmetric + asymmetric) boundaries as a function of rotation angle ξ and asymmetry angle η (for Ni only). Boundary character – twist, tilt or mixed – is defined by the orientation of the boundary plane relative to the rotation axis: twist/tilt boundaries have their planes perpendicular/parallel to the rotation axis and all other boundaries are considered mixed. Tilt boundaries are further classified as symmetric if the lattice planes parallel to the boundary are the same in both crystal grains and asymmetric otherwise. The lines at two borders of the surface at $\eta=0^o$ and $\eta=90^o$ in (C) are the same as the blue line in (B). To emphasize the symmetries, this plot shows two irreducible symmetry-equivalent zones described in figure 4.

Figure 7: GB energy variations in low-dimensional subsets within the 111 rotational set. The symbols are energies taken from the datasets of 388 boundaries with the assumed error bars of 5% while the lines and the surface shows the fit function itself. (**A**) Energies of twist boundaries as a function of rotation angle. (**B**) Energies of symmetric tilt boundaries as a function of rotation angle. (**C**) Energies of all tilt (symmetric + asymmetric) boundaries as a function of rotation angle ξ and asymmetry angle η (for Ni only). Boundary character–twist, tilt or mixed–is defined by the orientation of the boundary plane relative to the rotation axis: twist/tilt boundaries have their planes perpendicular/parallel to the rotation axis and all other boundaries are considered mixed. Tilt boundaries are further classified as symmetric if the lattice planes parallel to the boundary are the same in both crystal grains and asymmetric otherwise. The lines at two borders of the surface at $\eta=0^o$ and $\eta=120^o$ in (C) are the same as the blue line in (B). To emphasize the symmetries, this plot shows two irreducible symmetry-equivalent zones describedin figure 4.

Figure 8: GB energy variations in low-dimensional subsets within the 110 rotational set. The symbols are energies taken from the datasets of 388 boundaries with the assumed error bars of 5% while the lines and the surface shows the fit function itself. (**A**) Energies of twist boundaries as a function of rotation angle. (**B**) Energies of symmetric tilt boundaries as a function of rotation angle. (**C**) Energies of all tilt (symmetric + asymmetric) boundaries as a function of rotation angle ξ and asymmetry angle η (for Ni only). Boundary character–twist, tilt or mixed–is defined by the orientation of the boundary plane relative to the rotation axis: twist/tilt boundaries have their planes perpendicular/parallel to the rotation axis and all other boundaries are considered mixed. Tilt boundaries are further classified as symmetric if the lattice planes parallel to the boundary are the same in both crystal grains and asymmetric otherwise. The lines at two borders of the surface at $\eta=0^o$ and $\eta=180^o$ in (C) are the same as the blue line in (B). To emphasize the symmetries, this plot shows two irreducible symmetry-equivalent zones described in figure 4.

Figure 9: The atomistic energies of all 388 boundaries in all four elements reported in [6,7] plotted against the energies of the same boundaries computed from the interpolation function. The solid line corresponds to a perfect fit, while the dashed lines indicate the assumed 5% error bounds. For each metal the energies are scaled by the maximum energy computed over all 388 boundaries for the same metal.

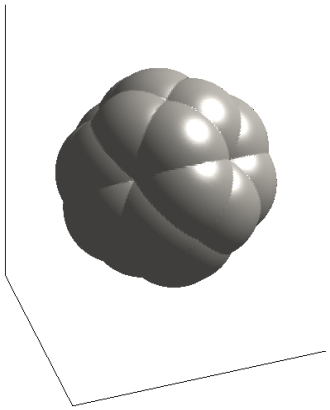

Figure 1: Density of broken 1NN bonds as a function of plane orientation.

a.

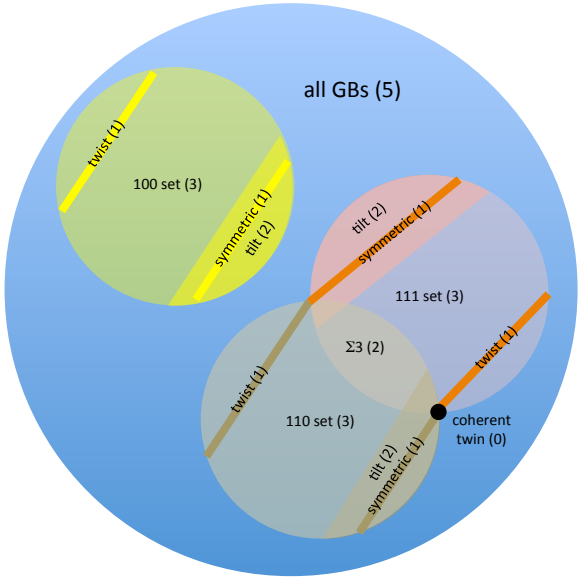
all GBs (5)
100 set (3)
twist (1)
symmetric (1)
tilt (2)
tilt (2)
symmetric (1)
111 set (3)
Σ3 (2)
twist (1)
twist (1)
110 set (3)
coherent twin (0)
tilt (2)
symmetric (1)

b.

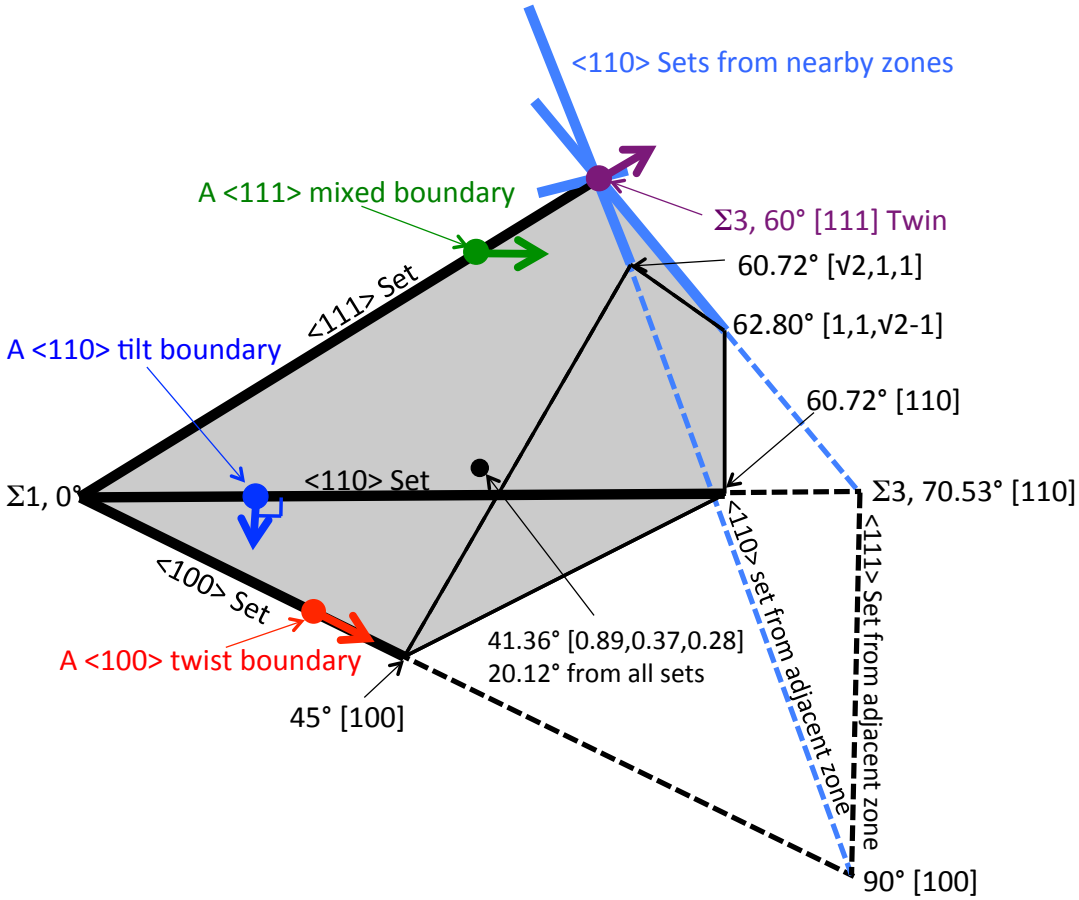
<110> Sets from nearby zones
A <111> mixed boundary
Σ3, 60° [111] Twin
60.72° [√2,1,1]
62.80° [1,1,√2-1]
<111> Set
A <110> tilt boundary
60.72° [110]
Σ1, 0°
<110> Set
Σ3, 70.53° [110]
<110> set from adjacent zone
<111> Set from adjacent zone
<100> Set
A <100> twist boundary
41.36° [0.89,0.37,0.28]
20.12° from all sets
45° [100]
90° [100]

Figure 2. a. An illustration of the set-theoretical relationship among the scaffolding sets. Dimensionality of each scaffolding set is given in parentheses. Special subsets of lower dimensionality are wholly included in the more general subsets of higher dimensionality. The subset of $\Sigma 3$ boundaries is the intersection of 111 and 110 sets: the small black circle within this subset is the $\Sigma 3$ (111)/(111) coherent twin boundary. All sets displayed in the figure also intersect at the $\Sigma 1$ "zero misorientation" boundary (not shown). **b.** Geometry of an arbitrary boundary in the 5D space can be represented as a point in Rodrigues space (representing the misorientation) with an attached unit vector (representing the boundary plane normal). We show four examples, superposed on the fundamental zone for misorientations in centrosymmetric cubic crystals. The scaffolding sets lie along the thick black and blue lines. The most remote point from the scaffolding sets is shown near the center of the fundamental zone.

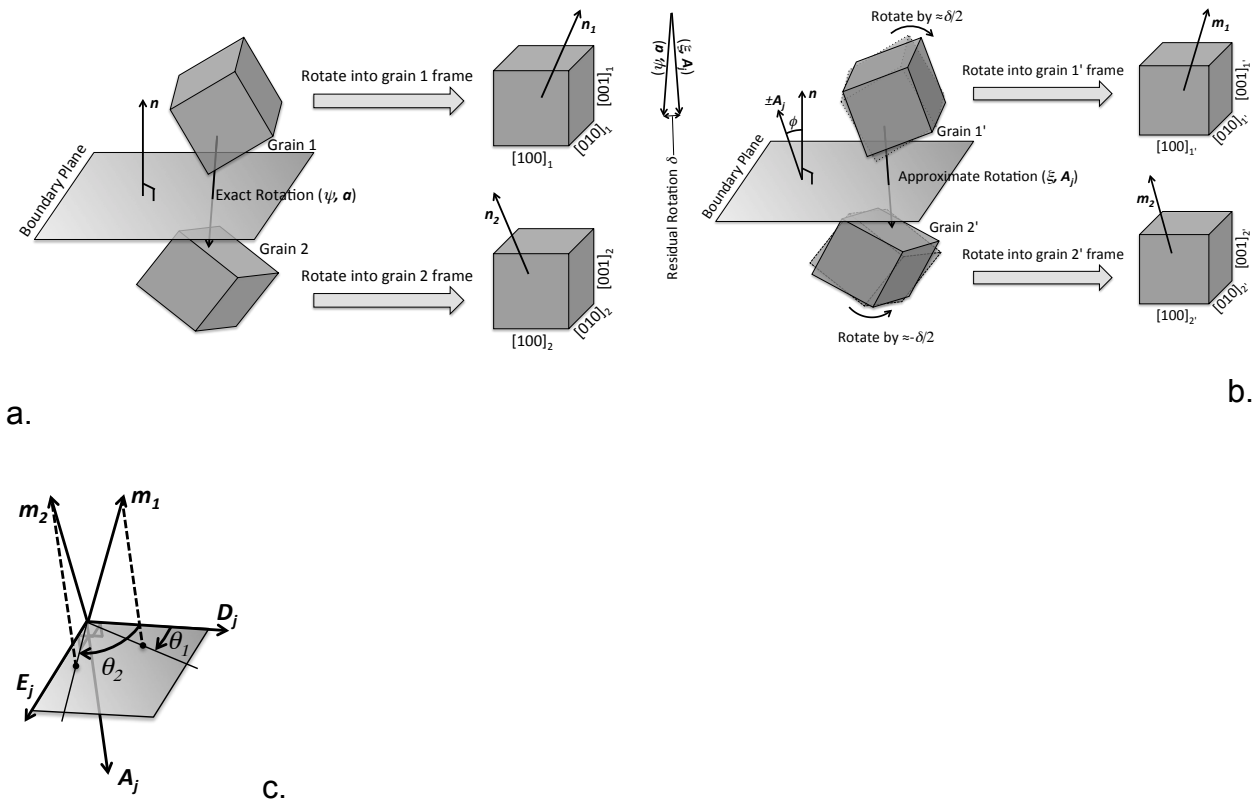

Figure 3: Geometry of grain boundaries: **a.** The axis-angle representation (ψ, ***a***) of the rotation and the boundary plane unit normal vectors $\boldsymbol{n_1}$ and $\boldsymbol{n_2}$ in each grain's reference frame; **b.** Finding the best match for boundary A among all boundaries obtainable by rotation about special axis $\boldsymbol{A_j}$. The closest match (ξ, $\boldsymbol{A_j}$) to the exact misorientation (ψ, ***a***) leaves a discrepancy that can be represented by a rotation over a small angle δ. Leaving the boundary plane fixed in the lab frame, each grain is rotated by approximately $\pm\delta/2$, defining new approximate grain orientations 1' and 2' with unit normals $\boldsymbol{m_1}$ and $\boldsymbol{m_2}$ expressed in the reference frames of these two grains; **c.** A Cartesian coordinate system ($\boldsymbol{A_j}$, $\boldsymbol{D_j}$, $\boldsymbol{E_j}$) is defined in a crystallographic reference frame, e.g. ($\boldsymbol{A_j}$, $\boldsymbol{D_j}$, $\boldsymbol{E_j}$) = ([100],[010],[001]) for each axis $\boldsymbol{A_j}$. $\boldsymbol{D_j}$ is always chosen to be a <100> or a <110> direction. The boundary plane normals in the approximating boundary are projected into the ($\boldsymbol{D_j}$, $\boldsymbol{E_j}$) plane, thus defining the angles θ_1 and θ_2.

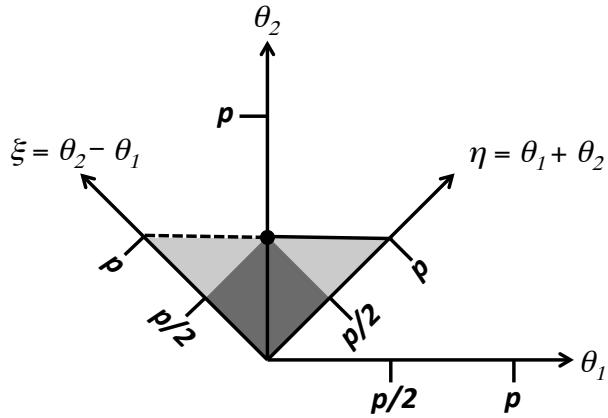

Figure 4: Variable transformation from (θ_1, θ_2) to (ξ, η) and reduction to a minimal symmetry-equivalent triangular zone (union of light gray and dark gray regions). By symmetry, all functions must be periodic in θ_1 and θ_2 with period *p* and possess mirror symmetry with respect to the ξ and η axes. The point marked with a dot has 2-fold rotation symmetry, thus the boundary segment shown in a dashed line is redundant. All other boundary segments are parts of the shaded irreducible zone. Twist boundaries are defined to have η = 0. While such symmetry reduction is applicable to all high-symmetry axes, the set of <111> tilt boundaries possesses an extra symmetry reducing the fundamental zone to the dark gray region.

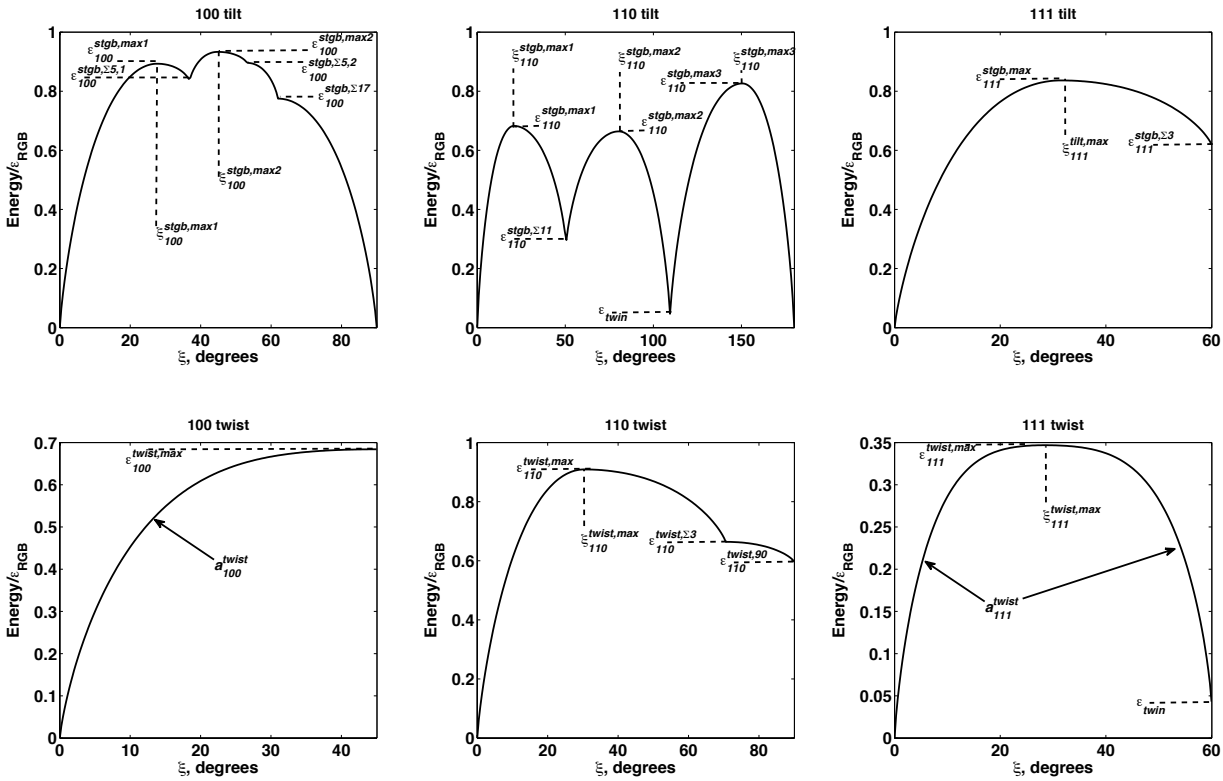

Figure 5: Parameterization of GB energy variations within special one-dimensional subsets of twist and symmetric tilt boundaries in the <100>, <110>, and <111> scaffolding sets. Numerical parameters (angles and scaled energies) defining the shapes of the one-dimensional functions are listed on the plots. Unless shown on the plot, parameters *a* defining the shape of the RSW functions are set to *a* = 0.5.

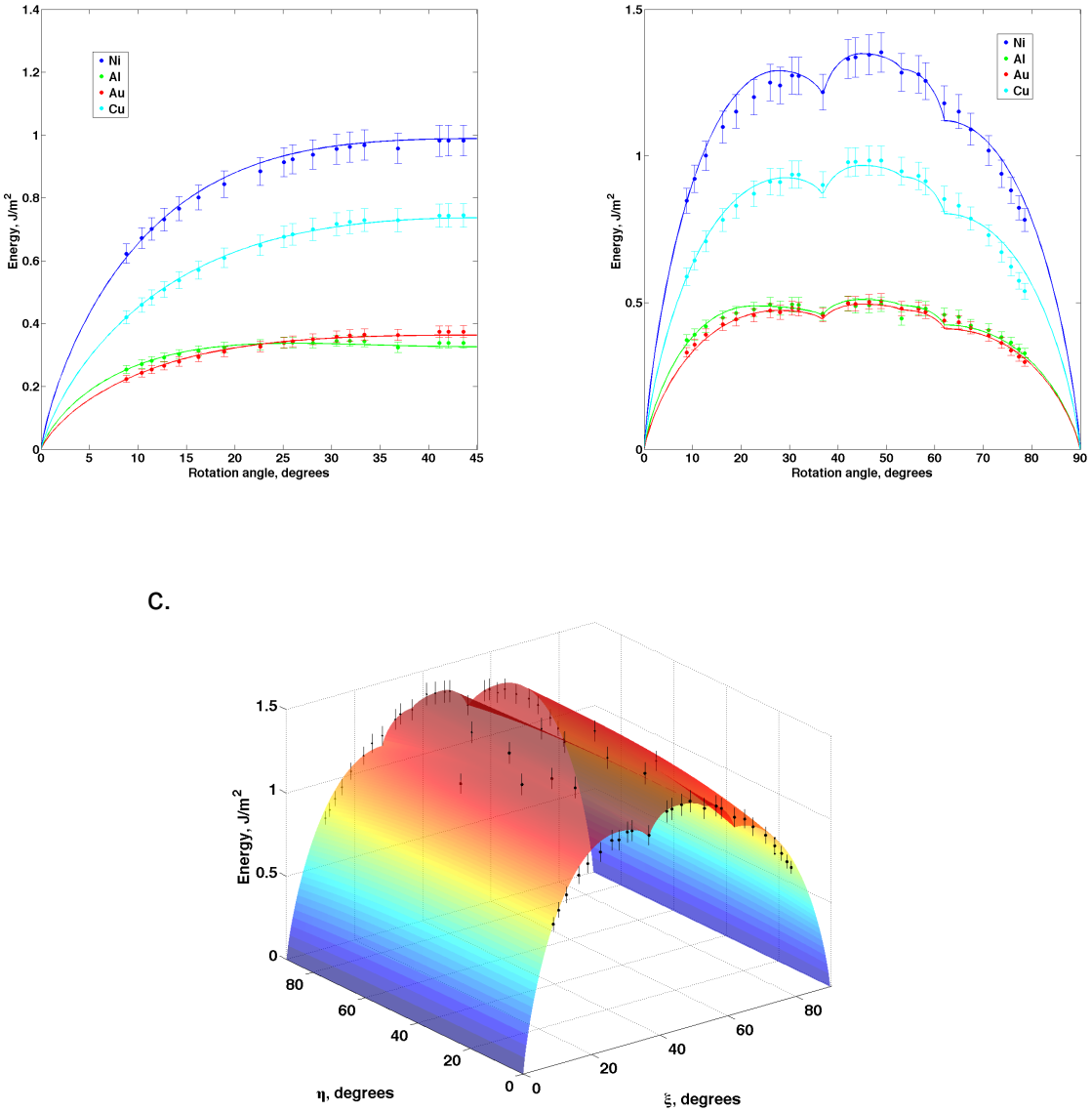

Figure 6: GB energy variations in low-dimensional subsets within the 100 rotational set. The symbols are energies taken from the datasets of 388 boundaries with the assumed error bars of 5% while the lines and the surface shows the fit function itself. (**A**) Energies of twist boundaries as a function of rotation angle. (**B**) Energies of symmetric tilt boundaries as a function of rotation angle. (**C**) Energies of all tilt (symmetric + asymmetric) boundaries as a function of rotation angle ξ and asymmetry angle η (for Ni only). Boundary character – twist, tilt or mixed – is defined by the orientation of the boundary plane relative to the rotation axis: twist/tilt boundaries have their planes perpendicular/parallel to the rotation axis and all other boundaries are considered mixed. Tilt boundaries are further classified as symmetric if the lattice planes parallel to the boundary are the same in both crystal grains and asymmetric otherwise. The lines at two borders of the surface at $\eta=0^o$ and $\eta=90^o$ in (C) are the same as the blue line in (B).

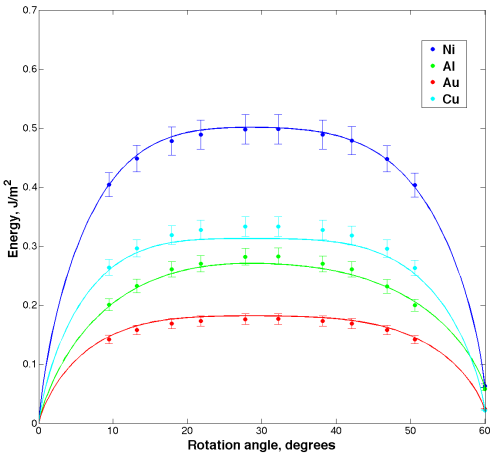

a.

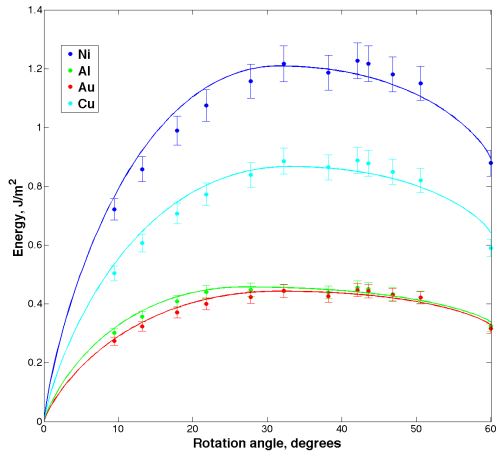

b.

c.

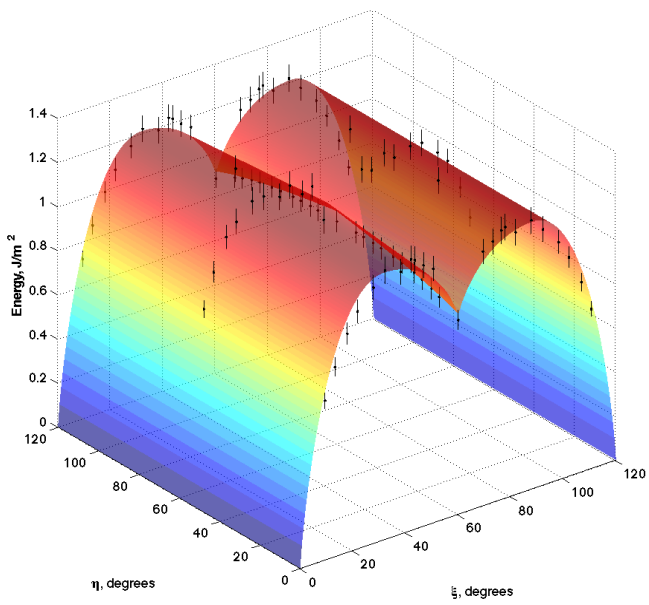

Figure 7: GB energy variations in low-dimensional subsets within the 111 rotational set. The symbols are energies taken from the datasets of 388 boundaries with the assumed error bars of 5% while the lines and the surface shows the fit function itself. (**A**) Energies of twist boundaries as a function of rotation angle. (**B**) Energies of symmetric tilt boundaries as a function of rotation angle. (**C**) Energies of all tilt (symmetric + asymmetric) boundaries as a function of rotation angle ξ and asymmetry angle η (for Ni only). Boundary character–twist, tilt or mixed–is defined by the orientation of the boundary plane relative to the rotation axis: twist/tilt boundaries have their planes perpendicular/parallel to the rotation axis and all other boundaries are considered mixed. Tilt boundaries are further classified as symmetric if the lattice planes parallel to the boundary are the same in both crystal grains and asymmetric otherwise. The lines at two borders of the surface at η=0° and η=120° in (C) are the same as the blue line in (B).

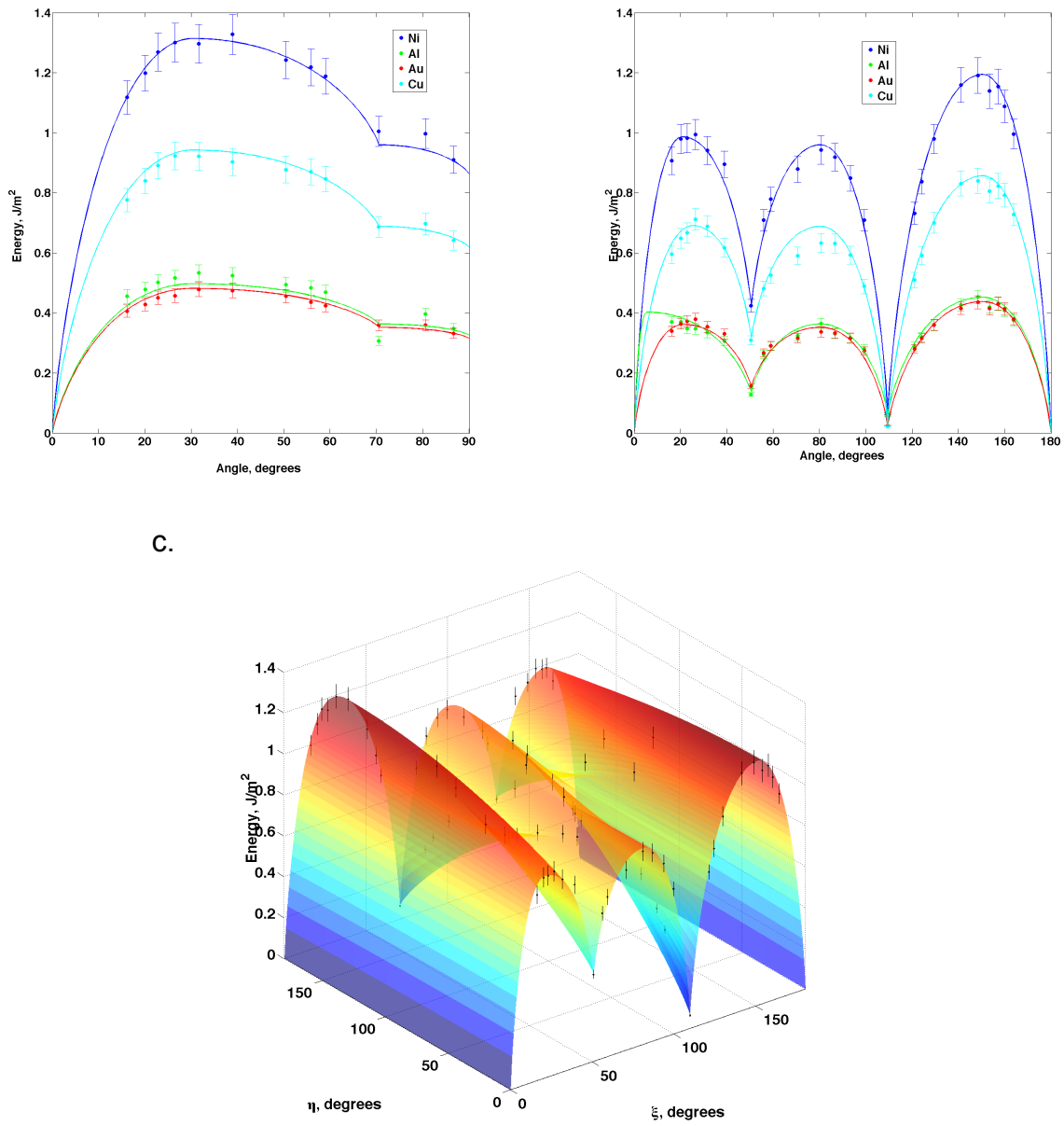

Figure 8: GB energy variations in low-dimensional subsets within the 110 rotational set. The symbols are energies taken from the datasets of 388 boundaries with the assumed error bars of 5% while the lines and the surface shows the fit function itself. (**A**) Energies of twist boundaries as a function of rotation angle. (**B**) Energies of symmetric tilt boundaries as a function of rotation angle. (**C**) Energies of all tilt (symmetric + asymmetric) boundaries as a function of rotation angle ξ and asymmetry angle η (for Ni only). Boundary character–twist, tilt or mixed–is defined by the orientation of the boundary plane relative to the rotation axis: twist/tilt boundaries have their planes perpendicular/parallel to the rotation axis and all other boundaries are considered mixed. Tilt boundaries are further classified as symmetric if the lattice planes parallel to the boundary are the same in both crystal grains and asymmetric otherwise. The lines at two borders of the surface at η=0° and η=180° in (C) are the same as the blue line in (B).

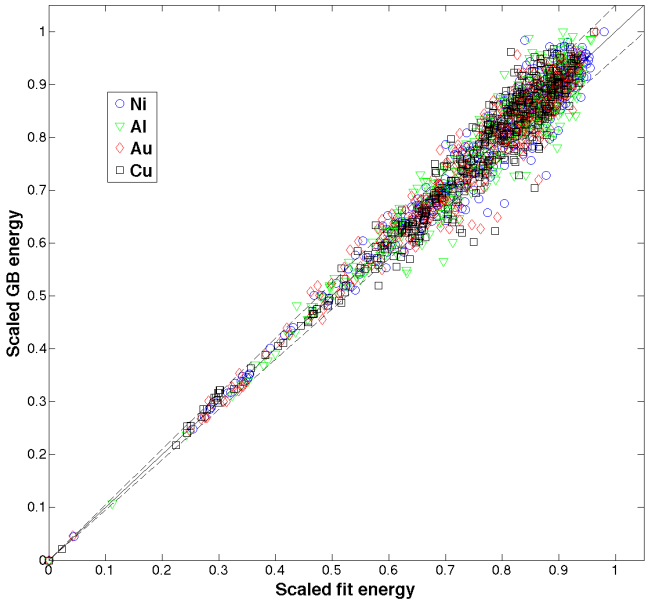

Figure 9: The atomistic energies of all 388 boundaries in all four elements reported in [6,7] plotted against the energies of the same boundaries computed from the interpolation function. The solid line corresponds to a perfect fit, while the dashed lines indicate the assumed 5% error bounds. For each metal the energies are scaled by the maximum energy computed over all 388 boundaries for the same metal.